A new linear forcing method for isotropic turbulence with controlled integral length scale

Jérémie Janin,[1,2] Fabien Duval,[1,a)] Christophe Friess,[2] and Pierre Sagaut[2]
[1)] *Institut de Radioprotection et de Sûreté Nucléaire (IRSN), Saint Paul Lez Durance, 13115 France*
[2)] *Aix-Marseille Univ., CNRS, Centrale Marseille, M2P2 Marseille, France*

(Dated: 14 April 2021)

Turbulence is a common feature to all flows that surround us. Despite its ubiquity, particularly in industrial flows, it is very difficult to provide a mathematical framework for the generation of turbulent eddies. Several methods have been proposed which are able to reproduce realistic features for velocity fluctuations, exhibiting proper space- and time-correlations. Focusing on physical space forcing, these methods are usually first evaluated upon sustained homogeneous isotropic turbulence by introducing a body force to the Navier-Stokes equations. Since the pioneering work of Lundgren, these techniques usually experience difficulties in predicting the integral length scale. The present study provides a forcing through a reconstruction approach which consists in building velocity fluctuations with a prescribed energy spectrum model. The proposed approach is assessed by performing large-eddy simulations of a sustained homogeneous isotropic turbulence in a triply periodic box. Properties of this forcing technique are discussed, drawing on both spatial and time correlations and also on the shape of energy spectrum together with the level of resolved turbulent kinetic energy. A special attention is put on the control of resolved turbulent energy. In this framework, an efficient selective forcing technique is derived, making use of spectral space features. The results show that the proposed approach allows to drive efficiently the resolved kinetic energy towards its target value while preserving the integral length scale independent of the domain size. It is observed that the resulting longitudinal length scale is overestimated by 13%, while the two-time correlations are recovered when using stochastic frequencies.

I. INTRODUCTION

Forcing techniques, for instance in large-eddy simulations (LES) methods have gained in importance over the past decade. A large part of their development is dedicated to sustain homogeneous turbulence with targeted statistical properties to study, for instance particle dispersion[1,2] or premixed combustion[3,4]. Forcing techniques can also be used to locally introduce velocity fluctuations in computations[5,6]. This allows to trigger turbulence when natural mechanisms (strong shear due to a geometrical singularity, ...) are absent or not sufficient to promote turbulence.

Forcing techniques consist usually in adding a volume force to the Navier-Stokes equations. This approach has been followed in either spectral[7,8] or physical[9,10] spaces, depending on the solving method for the Navier-Stokes equations. Forcing in spectral space is usually restricted on a limited wave number range which is located towards low wave numbers. This is motivated by the need to enrich only large-scale structures, without explicitly modifying the inertial subrange. On the other hand, physical space forcing usually lies in injecting energy over the full wave number range. Table I displays an overview of previous forcing methods in physical space. These methods refer to linear forcing techniques as the forcing term is linear in either the velocity (Lundgren's[10]) or a synthetic velocity (Schmidt and Breuer's[5]). In the following, we focus on approaches derived from the former and latter forcing techniques.

As previously stated, one way to perform physical forcing is to add a force to the Navier-Stokes equations which is linear in velocity. Such techniques are based on Lundgren's methodology[10] which is a simple and efficient way to sustain turbulence. Analysis of the turbulent kinetic energy budget shows that the term leading to turbulent production comes from $u_j' \partial_j \bar{u}_i$ (where $\bar{\cdot}$ stands for the ensemble average) in the transport equation for the fluctuating velocity component u_i'. This term vanishes for homogeneous isotropic flows, which motivated Lundgren to produce his "linearly forced isotropic turbulence" method in physical space by adding a forcing term proportional to the velocity. This method has two well-known shortcomings when applied to sustain isotropic homogeneous turbulence in a triply periodic box: *(i)* it generates important oscillations of the turbulent kinetic energy and *(ii)* the resulting integral length scale $L_{||}$, defined as $L_{||} = U_{rms}^3/\varepsilon$, depends on the domain size L_{box}, in practice $L_{||} \sim 0.2 L_{box}$. Recent improvements allow to circumvent these shortcomings by *(i)* introducing a modulation coefficient based on the turbulent kinetic energy or dissipation budget, that greatly reduces oscillations and substantially shortens the initial transient phase[1,11], and *(ii)* by employing filters that ensure a nearly unconstrained integral length scale which is independent of the domain size[12,13]. In most instances, the two aforementioned limitations are tackled separately, focusing on the control of either turbulent kinetic energy or integral length scale as noted in Table I.

In the present work, an alternate approach is investigated that consists in introducing synthetic velocity fluctuations through a linear-like forcing technique approach. Following a reconstruction approach[14], a homogeneous isotropic Gaussian synthetic turbulent velocity field is built and introduced in the Navier-Stokes equations. In other words, synthetic velocity fluctuations are added to the resolved velocity field promoting turbulence within the simulation. This is in line with the work of Schmidt and Breuer[5]. They proposed to add a

[a)] Author to whom correspondence should be addressed. Electronic email: fabien.duval@irsn.fr

TABLE I: Overview of introduced forcing techniques. $\langle . \rangle$ and $\tilde{.}$ represent respectively a temporal and spatial filter. $\hat{\tilde{.}}$ represents a double spatial filter, where the second filter is explicit. T denotes the turn-over time scale.

Source	Forcing term f_i	Remarks
Lundgren (2003)	$A\tilde{u}_i$	Constrained $L_{\|\|} \sim 19\% L_{box}$. Long transition to statistically stationary state $\sim 20T$
Carroll & Blanquart (2013)	$A\frac{k_r^\dagger}{k_r}\tilde{u}_i$	Constrained $L_{\|\|} \sim 19\% L_{box}$. Short transition to statistically stationary state $\sim 8T$
Mallouppas *et al.* (2013)	$\frac{\sqrt{k_r^\dagger}-\sqrt{k_r}}{\delta t\sqrt{k_r^\dagger}}u_i^s$	Very short transition to statistically stationary state $< T$
De Laage de Meux *et al.* (2015)	$A_{ij}\left(\tilde{u}_j-\hat{\tilde{u}}_j\right)+B_i$	Unconstrained $L_{\|\|}$. Short transition to statistically stationary state $\sim T$. Appropriate for anisotropic flows
Bassenne *et al.* (2016)	$\frac{\varepsilon - G\left[k_r - k_r^\dagger\right]}{2k_r T}\tilde{u}_i$	Constrained $L_{\|\|} \sim 19\% L_{box}$. Very short transition to statistically stationary state $< T$
Schmidt & Breuer (2017)	$\frac{\langle u_i^s \rangle}{T}$	Unconstrained $L_{\|\|}$. Prescribed two-point and two-time correlations are matched
Palmore Jr. & Desjardins (2018)	$A\frac{k_r^\dagger}{k_r}\hat{\tilde{u}}_i$	Unconstrained $L_{\|\|}$. Short transition to statistically stationary state $\sim T$

synthetic source term to the Navier-Stokes equations. In their work, this source term is expressed as the ratio between a synthetic velocity and a turn-over time scale. The synthetic velocity field is frozen, *i.e.* time independent, and is based on a digital filter approach[15]. The parameters of the digital filter procedure are randomly chosen at each time step and to obtain the targeted two-time correlations the synthetic velocity field is filtered. Their work was then taken over by De Nayer *et al.*[6] to improve prediction for a practical LES case.

In this study, an inverse Fourier approach is used to build the synthetic velocity field. This methodology, based on the work of Kraichnan[16], basically consists in writing the velocity field in the Fourier space and then summing different Fourier modes over a shell. The generated velocity field needs an energy spectrum model as input. Consequently, one has to specify a total kinetic energy as well as an integral length scale to set up the prescribed energy spectrum. Statistical properties such as two-point and two-time correlation functions depend strongly on the energy spectrum function. This suggests that the prescribed spectrum must be as close as possible to the considered physics. A careful choice of other variables (wave number, phase, ...) allows to ensure homogeneity and isotropy, along with a divergence-free field.

This frozen synthetic velocity field is well suited and mainly used to initialize simulations. Based on the work of Kraichnan, Fung *et al.*[17] provided an unfrozen synthetic velocity field, *i.e.* time dependent, introducing a prescribed time frequency which remains to be specified. Following Bailly *et al.*[18], one way is to prescribe a constant time frequency for all Fourier modes. More physics can be added to the model by means of *straining* or *sweeping* hypothesis. Time frequencies are driven by two distinct mechanisms, depending on whether large scales or small scales are considered. Favier *et al.*[19] highlighted the transition between *straining* and *sweeping* hypotheses. They validated that large scales follow the *straining* hypothesis while small scales verify the *sweeping* hypothesis. The *straining* hypothesis states that large scale frequencies only depend on size and energy of the larger eddies, whereas the *sweeping* hypothesis stipulates that small scales are advected by larger ones. As described by Favier *et al.*[19], using a random frequency that obeys a Gaussian distribution, smoothens the two-time synthetic velocity correlations. In this study, we show the impact of a random frequency on two-time velocity correlations.

In addition to recovering the prescribed length scale and the two-time correlations, the control of the resolved turbulent kinetic energy is of significant importance. A simple way for controlling the turbulent kinetic energy is to use a PI controller to trigger second order moments toward a targeted value as in the work of Spille-Kohoff and Kaltenbach[9]. Since their pioneer work, the method has been improved in particular by Laraufie *et al.*[20]. An other way is to introduce a modulation coefficient based on the turbulent kinetic energy budget[1,11]. For instance, Carroll and Blanquart[11] proposed a modified version of Lundgren's linear forcing method[10] by multiplying the forcing term by the control coefficient $k_r^\dagger/k_r$ as shown in Table I. This control aims at driving the kinetic energy k_r towards the targeted one $k_r^\dagger$. This has the effect of reducing both oscillations of the turbulent kinetic energy and the initial transient phase. Finding a modulation coefficient when applying a forcing based on the resolved velocity field is well suited but becomes challenging when adding a forcing based on synthetic velocity fluctuations to the Navier-Stokes equations. In this instance, Malloupas *et al.* proposed an ap-

proach that consists in multiplying the forcing term by the coefficient $(\sqrt{k_r^\dagger} - \sqrt{k_r})/\delta t \sqrt{k_r^\dagger}$, where δt is the computational time step. In the present study, two novel strategies for monitoring the turbulent kinetic energy are proposed. First, a modulation coefficient is proposed based on the kinetic energy budget with an estimate of the production of turbulent kinetic energy related to the forcing method. Secondly, a control that mimics spectral forcing techniques, is derived. The aim of this method is to control the resolved kinetic energy by summing a specific number of Fourier modes, *i.e.* injecting a specific amount of kinetic energy. The proposed approach is tested upon homogeneous and isotropic turbulence (HIT), today's state-of-start approach to benchmark and investigate a forcing method's characteristics.

The structure of the paper is as follows. In Section II the reconstruction approach is presented. The formulation of the synthetic velocity is described as well as the energy spectra chosen in this study. Besides, the benefit of a stochastic frequency on the synthetic two-time correlations, is explained. Section III is dedicated to the kinetic energy monitoring. In Section IV, results of the proposed forcing upon HIT in 2π-triply periodic box, are presented.

II. RECONSTRUCTION APPROACH

The proposed forcing technique consists in introducing velocity fluctuations in the filtered Navier-Stokes equations following a reconstruction approach[14]. This approach consists roughly in substituting the resolved velocity by the sum of the resolved velocity and a synthetic component u_i^s. This operation leads to new terms in the filtered Navier-Stokes equations but we assume here that all these terms can be neglected at least for HIT except for the unsteady term, leading to the following forcing:

$$\frac{\partial \tilde{u}_i}{\partial t} + \tilde{u}_j \frac{\partial \tilde{u}_i}{\partial x_j} = -\frac{1}{\rho}\frac{\partial \tilde{p}}{\partial x_i} + \nu \frac{\partial^2 \tilde{u}_i}{\partial x_j \partial x_j} - \frac{\partial \tau_{ij}}{\partial x_j} - \frac{\partial u_i^s}{\partial t} \qquad (1)$$

in which $\tilde{u}_i$, $\tilde{p}$, ν and τ_{ij} are respectively the resolved velocity, the resolved pressure, the kinematic viscosity, and the subgrid tensor. This approach is formally equivalent to the method proposed by Schmidt and Breuer[5] in which the last term on the right hand side of Eq.(1) plays the role of the forcing term. In their approach, the synthetic velocity is frozen, *i.e.* time independent. In order to recover the two-time correlations a relaxation time based on Taylor's hypothesis is used instead of the temporal derivative. Then the synthetic velocity field is preliminary filtered by a temporal exponential moving average before being injected into the computation. The resulting forcing writes as the ratio of a filtered stochastic synthetic velocity $\hat{u}_i^s$, prescribed randomly at each time step by a specified characteristic turbulent time scale. The forcing term is therefore expressed in a similar way as in the linear forcing approach[1,10,11,21]:

$$\frac{\partial \tilde{u}_i}{\partial t} + \tilde{u}_j \frac{\partial \tilde{u}_i}{\partial x_j} = -\frac{1}{\rho}\frac{\partial \tilde{p}}{\partial x_i} + \nu \frac{\partial^2 \tilde{u}_i}{\partial x_j \partial x_j} - \frac{\partial \tau_{ij}}{\partial x_j} + \frac{\hat{u}_i^s}{T} \qquad (2)$$

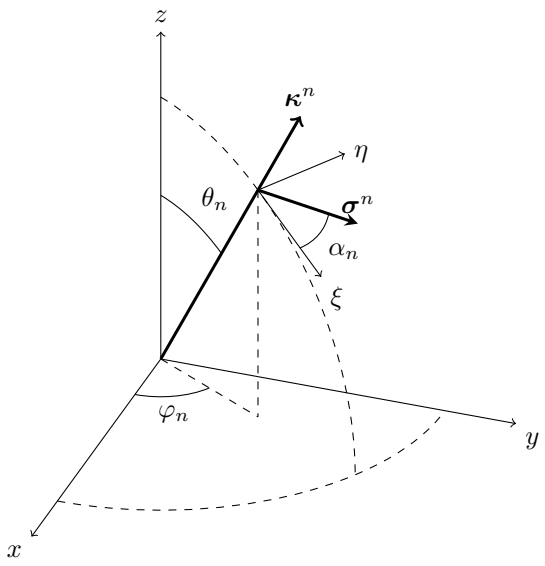

FIG. 1: Wave vector geometry of the n^{th} Fourier mode.

The present approach uses an unfrozen synthetic velocity field through the introduction of a stochastic time frequency. More details are given in Sec. II A.

A. Synthetic velocity field

The synthetic velocity used in this study originates from the work of Kraichnan[16] which has been later extended by Fung *et al.*[17], providing an unfrozen synthetic velocity field. The method is briefly recalled hereafter. The starting point of this approach is the inverse Fourier transform of the velocity field:

$$\boldsymbol{u}^s(\boldsymbol{x},t) = \int_{-\infty}^{\infty}\int_{-\infty}^{\infty} \left[\hat{u}(\boldsymbol{\kappa},\omega) e^{\imath\psi(\boldsymbol{\kappa},\omega)} \boldsymbol{\sigma}(\boldsymbol{\kappa},\omega)\right] e^{\imath(\boldsymbol{\kappa}\cdot\boldsymbol{x}+\omega t)} d\boldsymbol{\kappa} d\omega \qquad (3)$$

Considering only one frequency for each wave length, Eq. (3) is then discretized in N random Fourier modes on a half-spherical spectral space:

$$\boldsymbol{u^s}(x,t) = 2\sum_{n=1}^{N} \hat{u}_n \cos(\boldsymbol{\kappa}^n \cdot \boldsymbol{x} + \psi_n + \omega_n t)\boldsymbol{\sigma}^n \qquad (4)$$

where $\hat{u}_n$, ψ_n, $\boldsymbol{\sigma}^n$ and ω_n correspond respectively to the amplitude, the phase, the direction and the time frequency of the n^{th} Fourier mode related to the wave vector $\boldsymbol{\kappa}^n$. The wave vector $\boldsymbol{\kappa}^n$ is randomly chosen on a half spherical shell with radius $\kappa_n = |\boldsymbol{\kappa}^n|$ to ensure statistical isotropy. Using spherical coordinates$(\kappa_n, \phi_n, \theta_n)$, as shown in Fig. 1, its components are calculated as:

$$\kappa_1^n = \kappa_n \sin(\theta_n)\cos(\varphi_n) \qquad (5)$$

$$\kappa_2^n = \kappa_n \sin(\theta_n)\sin(\varphi_n) \qquad (6)$$

$$\kappa_3^n = \kappa_n \cos(\theta_n) \qquad (7)$$

where θ_n, $0 \le \theta_n \le \pi$ and φ_n, $0 \le \varphi_n \le \pi$ are random angles defined for the n^{th} mode. Requiring that the probability of a

TABLE II: Probability density functions of random variable

Pdf	Interval
$P(\varphi_n) = 1/\pi$	$0 \leq \varphi_n \leq \pi$
$P(\theta_n) = \sin(\theta_n)/2$	$0 \leq \theta_n \leq \pi$
$P(\alpha_n) = 1/(2\pi)$	$0 \leq \alpha_n \leq 2\pi$
$P(\psi_n) = 1/(2\pi)$	$0 \leq \psi_n \leq 2\pi$

randomly selected direction of a wave vector to be the same for all dS on the half shell of the sphere whose radius is κ_n, leads to:

$$p(\kappa_n)d\kappa_n = \frac{dS}{2\pi\kappa_n^2} \tag{8}$$

$$p(\theta_n)d\theta_n p(\varphi_n)d\varphi_n = \frac{\kappa_n d\theta_n \kappa_n \sin(\theta_n)d\varphi_n}{2\pi\kappa_n^2} \tag{9}$$

The divergence-free condition $\nabla \cdot \boldsymbol{u}^s = 0$ implies that $\boldsymbol{\kappa}^n$ is orthogonal to $\boldsymbol{\sigma}^n$. As a result, the unit vector $\boldsymbol{\sigma}^n$ is given by:

$$\sigma_1^n = \cos(\varphi_n)\cos(\theta_n)\cos(\alpha_n) - \sin(\varphi_n)\sin(\alpha_n) \tag{10}$$

$$\sigma_2^n = \sin(\varphi_n)\cos(\theta_n)\cos(\alpha_n) + \cos(\varphi_n)\sin(\alpha_n) \tag{11}$$

$$\sigma_3^n = -\sin(\theta_n)\cos(\alpha_n) \tag{12}$$

The phase ψ_n is randomly chosen to satisfy spatial homogeneity. The probability density functions for the parameters φ_n, θ_n,α_n and ψ_n are given in Table II. Besides, the amplitude is written as $\hat{u}_n = \sqrt{E(\kappa_n)\delta\kappa_n}$, where $E(\kappa)$ is a prescribed energy spectrum and $\delta\kappa_n$ denotes the wave number step of the n^{th} mode in the interval $[\kappa_1, \kappa_N]$. For a logarithmic discretization, κ_n and $\delta\kappa_n$ are simply given by:

$$\delta\kappa_n = \frac{\log(\kappa_N) - \log(\kappa_1)}{N}, \quad \kappa_n = e^{(\log(\kappa 1) + n\delta\kappa_n)} \tag{13}$$

This allows a better discretization in the lower wave number range corresponding to the larger energy-containing eddies rather than a linear discretization[22,23]. Using statistical properties of the prescribed probability density functions, the synthetic kinetic energy is defined as:

$$k_s = \sum_{n=1}^{N} \hat{u}_n^2 = \int_0^{\kappa_{cut}} E(\kappa)d\kappa \tag{14}$$

in which κ_{cut} is the cut off number of the simulation. Similarly, one can show that the moments of the synthetic velocity verify a Gaussian distribution with zero mean and variance equal to $\overline{u_i^s u_j^s} = \frac{2}{3}k_s\delta_{ij}$ where the over bar represents a statistical averaging. The frequency ω_n is defined as:

$$\omega_n = \sqrt{\frac{\pi}{2}}\frac{\lambda_n}{T} = \lambda_n \breve{\omega}_n \tag{15}$$

in which T corresponds to the prescribed turn-over time scale and λ is a normal random variable which could be set to be deterministic, *i.e.* $\lambda \sim \mathcal{N}(\lambda_m, \lambda_\sigma = 0)$ or stochastic, *i.e.* $\lambda \sim \mathcal{N}(\lambda_m, \lambda_\sigma > 0)$. The turn-over time scale T is mode independent and therefore its corresponding frequency $\omega = \breve{\omega}_n$ is referred to as constant frequency.

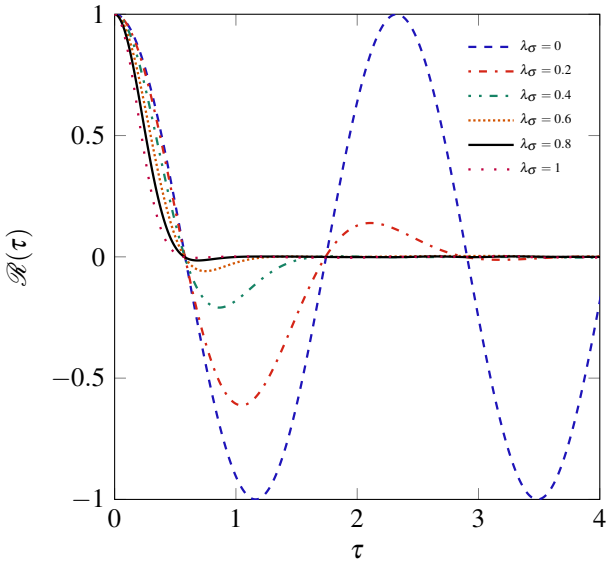

FIG. 2: Two-time correlation functions of the synthetic velocity u_i^s for different Gaussian distributions $\lambda \sim \mathcal{N}(\lambda_m = 0.6, \lambda_\sigma)$. Calculated from Eq 16.

Rather than using a deterministic value for λ, the use of a Gaussian distribution plays a crucial role in recovering two-time correlations of the synthetic velocity u_i^s. Indeed, a stochastic value for λ prevents from strong oscillations on the behavior of the two-time correlation function[19]. When looking at the two time correlation function, and considering the frequency $\omega_n = \lambda_n\omega$, we get:

$$\mathscr{R}(\tau) = \frac{\overline{u_1^s(t)u_1^s(t+\tau)}}{\overline{u_1^s u_1^s}} = \frac{2}{k_s}\sum_{n=1}^{N}\hat{u}_n^2\overline{\cos(\lambda_n\omega\tau)} \tag{16}$$

where τ is the separation time. By using the central limit theorem and by ensuring in practice that $N > 30$, Eq. (16) becomes:

$$\mathscr{R}(\tau) \underset{N\to+\infty}{\longrightarrow} \frac{2}{k_s}\sum_{n=1}^{N}\hat{u}_n^2 exp\left(-\frac{1}{2}(\lambda_m^2 + \lambda_\sigma^2)\omega^2\tau^2\right) \tag{17}$$

In order not to alter the correlation function, one needs to ensure that $(\lambda_m^2 + \lambda_\sigma^2) = 1$. In addition, as explained by Favier *et al.*[19], the condition $\lambda_\sigma > \lambda_m$ must be satisfied to avoid negative loops as depicted in Fig. 2. The two following Gaussian distributions are assessed in this study:

$$\lambda \sim \begin{cases} \mathcal{N}(\lambda_m = 1, \lambda_\sigma = 0) & \text{deterministic} \\ \mathcal{N}(\lambda_m = 0.6, \lambda_\sigma = 0.8) & \text{stochastic} \end{cases} \tag{18}$$

The $\sqrt{\frac{\pi}{2}}$ factor in the definition of the frequency ω Eq. (15) allows to theoretically recover the prescribed turn-over time scale T. Indeed, the turn-over time scale is defined as the integration of the two time correlation function. Integrating Eq. (17) from zero to infinity leads to the recovery of a factor $\frac{\pi}{2}$ in the numerator which is a classical Gaussian integration result. Therefore, without this coefficient the turn-over time scale would be increased.

B. Energy spectrum

Two different spectra are used to carry out this study. The choice is made to use the Passot-Pouquet (PP) energy spectrum which provides a description of the largest scales and the von Kármán-Pao (VKP) energy spectrum which gives a description of the largest scale as well as the smallest ones. First, the PP energy spectrum reads as:

$$E_1(\kappa) = \alpha_e k L_e (\kappa L_e)^4 \exp -2(\kappa L_e)^2 \tag{19}$$

where L_e is the wavelength associated with κ_e responsible for the most energetic eddies. In other words, $E(\kappa)$ reaches its peak at $\kappa = \kappa_e$. This spectrum only represents large eddies while the inertial range is omitted, thus a coarse grid is sufficient to recover all wave numbers containing energy. L_e is related to the integral length scale $L_{||}$ as:

$$L_e = \alpha_L L_{||} \tag{20}$$

The coefficient α_e is found from the definition of the kinetic energy:

$$k = \int_0^\infty E(\kappa) d\kappa \tag{21}$$

From the definition of the integral length scale for an isotropic homogeneous turbulence α_L is recovered:

$$L_{||} = \frac{3\pi}{4k} \int_0^\infty \frac{E(\kappa)}{\kappa} d\kappa \tag{22}$$

Therefore, we obtain:

$$\alpha_e = \frac{32}{3}\sqrt{\frac{2}{\pi}} \approx 8.511, \quad \alpha_L = \frac{1}{\sqrt{2\pi}} \approx 0.3989 \tag{23}$$

The second model for the energy spectrum function corresponds to the von Kármán-Pao (VKP) energy spectrum given by:

$$E_2(\kappa) = \frac{2}{3}\alpha_e k L_e \frac{(\kappa L_e)^4}{[(\kappa L_e)^2 + 1]^{17/6}} \exp\left(-2(\kappa L_\eta)^2\right) \tag{24}$$

where L_η corresponds to κ_η and represents the Kolmogorov scale, *i.e.* the most dissipative eddies:

$$L_\eta = \left(\frac{\nu^3}{\varepsilon}\right)^{(1/4)} \tag{25}$$

This spectrum is in agreement with Kolmogorov's "$-5/3$" power-law and therefore reproduces the inertial subrange. The maximum occurs at $\sqrt{12/5}\kappa_e$. As seen previously, the coefficients α_E and α_L are determined respectively by definitions of kinetic energy (Eq. (21)) and integral length scale (Eq. (22)). For integration, the exponential part of the spectrum is neglected since for small κL_η, $f_\eta = \exp\left(-2(\kappa L_\eta)^2\right)$ tends to unity[24]. As a result we get

$$\alpha_e = \frac{55}{9\sqrt{\pi}} \frac{\Gamma(5/6)}{\Gamma(1/3)} \approx 1.453, \quad \alpha_L = \frac{\Gamma(1/3)}{\sqrt{\pi}\Gamma(5/6)} \approx 1.339 \tag{26}$$

Here, note that coefficients α_L and α_e are approximated by numerical integration. This allows to ensure a proper kinetic energy k and integral length scale $L_{||}$

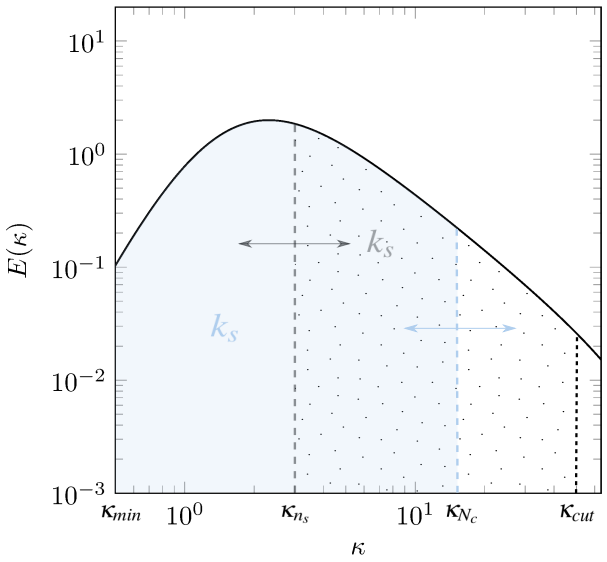

FIG. 3: Selective forcing scheme. Blue area: forcing starts from the lowest wave number κ_{min} to the time depending wave number κ_{N_c}. Dotted area: Forcing starts from the time depending wave number κ_{n_s} to the cut off wave number κ_{cut}.

III. KINETIC ENERGY MONITORING

The resolved kinetic energy k_r has to be controlled to ensure that it reaches the target filtered kinetic energy $k_r^\dagger$. In the following, we present two strategies for monitoring the resolved kinetic energy, both based on the turbulent kinetic energy budget that reads:

$$\frac{\partial k_r}{\partial t} = -\varepsilon - \overline{u_i \frac{\partial u_i^s}{\partial t}} \tag{27}$$

in which u_i, k_r and ε represents respectively the large scale velocity fluctuation, the resolved turbulent kinetic energy and the total dissipation which is the sum of the resolved and the sub-grid scale (SGS) dissipation $\varepsilon = \varepsilon_r + \varepsilon_{SGS}$. The first method uses a modulation coefficient, which is calibrated in such a way that the target dissipation is balanced by the synthetic production. The second method uses a selective forcing technique, which is an attempt to mimick spectral space forcing, with a selection of a given number of modes over which the synthetic velocity is computed. It should be recalled that the synthetic velocity is parametrized by the target total turbulent kinetic energy and the target integral length scale through the formulation for the energy spectrum. Here, the target resolved turbulent kinetic energy is directly linked to the target total kinetic energy $k^\dagger$ leading to the definition of the ratio $r = k_r^\dagger / k^\dagger$. This ratio is estimated using the formulation of the considered energy spectrum model.

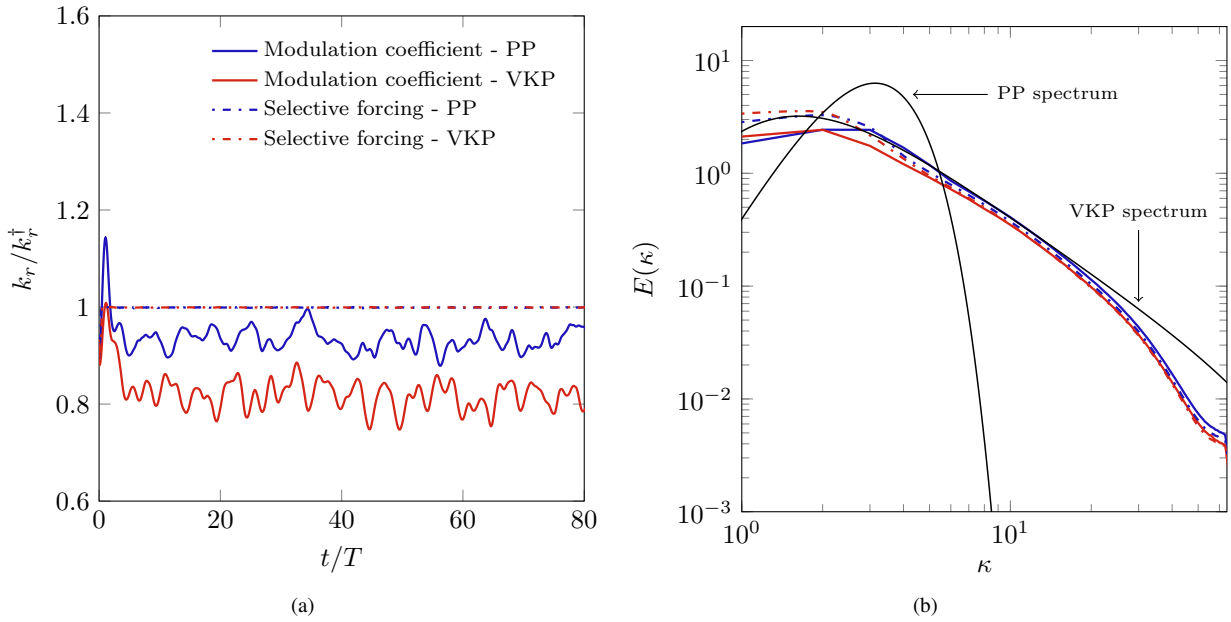

(a) (b)

FIG. 4: Comparison between the two forcing techniques: modulation coefficient A and selective forcing. Results are presented for the two studied energy spectrum: Passot-Pouquet (PP) and von Kármán-Pao (VKP) energy spectrum. (a) Time evolution of the resolved kinetic energy and (b) mean energy spectra averaged over the period of time $t \in [8T : 80T]$. Plain lines depict the analytical energy spectra.

A. Modulation coefficient

Adding a modulation coefficient A to the forcing term in the momentum equations Eq. (1) leads to rewrite Eq. (27) as:

$$\frac{\partial k_r}{\partial t} = -\varepsilon - A\overline{u_i \frac{\partial u_i^s}{\partial t}} \tag{28}$$

The synthetic production term $P^s = -\overline{u_i \frac{\partial u_i^s}{\partial t}}$ can be written as:

$$P^s = -\omega\overline{\left[u_i \frac{1}{\omega}\frac{\partial u_i^s}{\partial t}\right]} = \frac{\beta}{\omega}\overline{\left(\frac{\partial u_i^s}{\partial t}\right)^2} \tag{29}$$

where β is a scalar. In practice, the estimation of β is somewhat challenging, thus it is empirically set to the value 0.5. Using the expression for the synthetic velocity in Eq. (4), we obtain:

$$P^s = 2\beta\omega\sum_{n=1}^{N}\hat{u}_n^2\lambda_n^2 \tag{30}$$

Hence, when the statistically steady state is reached, the right-hand side of the kinetic energy budget Eq. (28) cancels and this allows the coefficient to be expressed as:

$$A = \frac{\varepsilon^\dagger}{2\beta\omega\sum_{n=1}^{N}\hat{u}_n^2\lambda_n^2} \tag{31}$$

in which $\varepsilon^\dagger$ corresponds to the target total dissipation. In the case of a deterministic λ, Eq. (31) simplifies to:

$$A = \frac{\varepsilon^\dagger}{2\beta\omega k_s} \tag{32}$$

This is very similar to Lundgren's approach[10] but with the resolved kinetic energy replaced by the synthetic kinetic energy k_s in the resulting forcing term. It is worth noticing that this modulation coefficient method acts as a passive control device. Moreover, it is strongly dependent on the value of the coefficient β. A better performance can be achieved with an active control method, as presented in the following section.

B. Selective forcing

With the present method, the amount of energy to be injected into the simulation, is quantified through first principle considerations. At each time step, enough energy must be injected to *(i)* compensate dissipation and *(ii)* drive the computed resolved turbulent kinetic energy k_r towards its target value $k_r^\dagger$. As a result, one can split the production term P^s induced by the synthetic velocity into a compensation of the dissipation P^{sd} and a dynamic control part P^{sc}. This approach naturally leads to the selective forcing because P^s/ω is a sum of discretized energies which can easily be adjusted to the kinetic energy that has to be injected, mimicking spectral space forcing. In order to determine the amount of energy to be injected, Eq. (27) is integrating between t and $t+\delta t$:

$$k_r(t+\delta t) - k_r(t) = -\varepsilon(t)\delta t + (P^{sd}(t) + P^{sc}(t))\delta t \tag{33}$$

where δt is an arbitrarily short time scale, e.g. the computational time step. As postulated, the production term P^{sd} must balance the total dissipation and is then equal to the target dissipation when the statistical stationary regime is reached. Since the production term P^{sd} balances the target dissipation

and requiring that the resolved kinetic energy reaches the targeted kinetic energy $k_r^\dagger$, the control part can be expressed as:

$$P^{sc}(t) = \frac{k_r^\dagger - k_r(t)}{\delta t} \tag{34}$$

By expressing $P^s = P^{sd} + P^{sc}$ with Eq. (30) and using Eq. (34), the amount of energy to be injected writes:

$$\sum_{n_s}^{N_c} \hat{u}_n^2 \lambda_n^2 = \frac{\varepsilon^\dagger}{2\beta\omega} + \frac{k_r^\dagger - k_r(t)}{2\beta\delta t\omega} \tag{35}$$

in which $n_s \in [1:N]$ and $N_c \in [1:N]$ are the lower and upper limit Fourier modes that satisfy Eq. (35). A specific wave number range can be selected by either summing upwards starting from the lowest wave number considered or downwards starting from the cut off wave number as illustrated in Fig. 3, *i.e.* this forcing may be performed either at large or small scales. Typically, when $n_s = 1$ and $N_c << N(\kappa_{cut})$ this mimics spectral space forcing at low wave numbers. In any case, the kinetic energy injected into the simulation must meet the condition defined by Eq. (35).

IV. FORCING APPLIED TO HOMOGENEOUS ISOTROPIC TURBULENCE

In this section, we test the robustness and the efficiency of the proposed approach upon homogeneous isotropic turbulence (HIT). Two strategies relating to the constant frequency ω of the synthetic velocity are investigated: *(i)* deterministic value for all modes, *(ii)* varying randomly from one mode to another following a Gaussian distribution. The reader is referred to Eq. (18) for the two Gaussian distributions used in this study. Then, we investigate the influence of grid resolution on important features of turbulence. The last part of this section provides an insight of the versatility of the proposed methodology by testing a more realistic frequency.

A. Numerical set up

The proposed approach is assessed by performing large-eddy simulations of a sustained homogeneous isotropic turbulence at $Re_\lambda = 90$ in a triply periodic box of size $L_{box} = 2\pi$. This case has been chosen considering previous investigation of linear forcing such as Carroll and Blanquart[11], Rosales and Meneveau[21], and Bassenne et. al[1] among others. The same procedure as in Sec. II A is used for initialization with $N = 200$ modes. The same number of mode is used for the synthetic forcing. Simulation results are obtained using the open-source generic CFD solver library CALIF^{3}S[25] (for Components Adaptive Library For Fluid Flow Simulations). Time discretization is performed by using a fractional step algorithm that consists in a pressure correction method. Space discretization is performed by using a staggered finite volume scheme for which scalar unknowns are located at cell centers while the velocity is located at cell faces. The numerical scheme is discretely kinetic energy conserving and corresponds to a centered second-order spatial discretization of both convective and diffusive fluxes together with the semi-implicit Crank-Nicolson time scheme[26]. The time step is fixed according to the CFL based on the prescribed root mean square (rms) velocity and the mesh size to be 0.1.

TABLE III: Summary table of study parameters

Parameters	Unity	$L_{\|\|} = 0.5m$	$L_{\|\|} = 0.8m$	$L_{\|\|} = 1.19m$
$L_{\|\|}/L_{box}$	-	8%	13%	19%
Re_λ	-	71	90	110
k	$m^2.s^{-2}$	17.1	17.1	17.1
$\varepsilon^\dagger$	$m^2.s^{-3}$	77.2	48.2	32.3
ν	$m^2.s^{-1}$	0.005	0.005	0.005
ρ	$kg.m^{-3}$	1.2	1.2	1.2
$\kappa_{max}L_\eta$	-	0.41	0.46	0.50

The numerical results are obtained with a dynamic Smagorinsky subgrid-scale model and a mesh containing $N^3 = 128^3$ grid points. The density is fixed to $\rho = 1.2\ kg.m^{-3}$ and the viscosity is equal to $\nu = 0.005\ m^2s^{-1}$. The grid resolution is such that $\kappa_{max}L_\eta = 0.46$, meaning that eddies with a size above six times the Kolmogorov scale are resolved. The target total dissipation is defined as $\varepsilon^\dagger = U_{rms}^3/L_{||}$ where $U_{rms} = \sqrt{2/3k^\dagger}$ is the rms velocity. Besides the studied length scale $L_{||} = 13\%L_{box}$, two different length scales are tested in this study. The corresponding simulation parameters are summarized in Table III. For the following results, all the statistic quantities considered (spectrum, two-point and two-time correlation) are averaged over at least 100 saves during 70 times the turn-over time scale T (Eq. (36)) for each case.

B. Constant frequency

As mentioned in Section II, the present approach is studied using a constant turn-over time scale T defined as:

$$T = \frac{k^\dagger}{\varepsilon^\dagger} \tag{36}$$

A comparison is made between a forcing with the modulation coefficient A and the proposed selective forcing starting from low wave numbers $\kappa_{min} = 0.01\kappa_e$. The consequences of the spectrum choice are shown hereafter by looking separately at the two proposed distributions of λ, the deterministic and stochastic one.

1. Deterministic frequency

In this section, we investigate the influence of a deterministic λ as referred in Eq. (18). Fig. 4a shows the time evolution of the resolved kinetic energy and their associated energy spectra average over the period of time $t \in [8T : 80T]$ are depicted in Fig. 4b. In the first place, it is worth noting that spectra have all a very similar inertial subrange. The main observed differences take place at large scales. In this area both spectra resulting from simulations with modulation coefficient

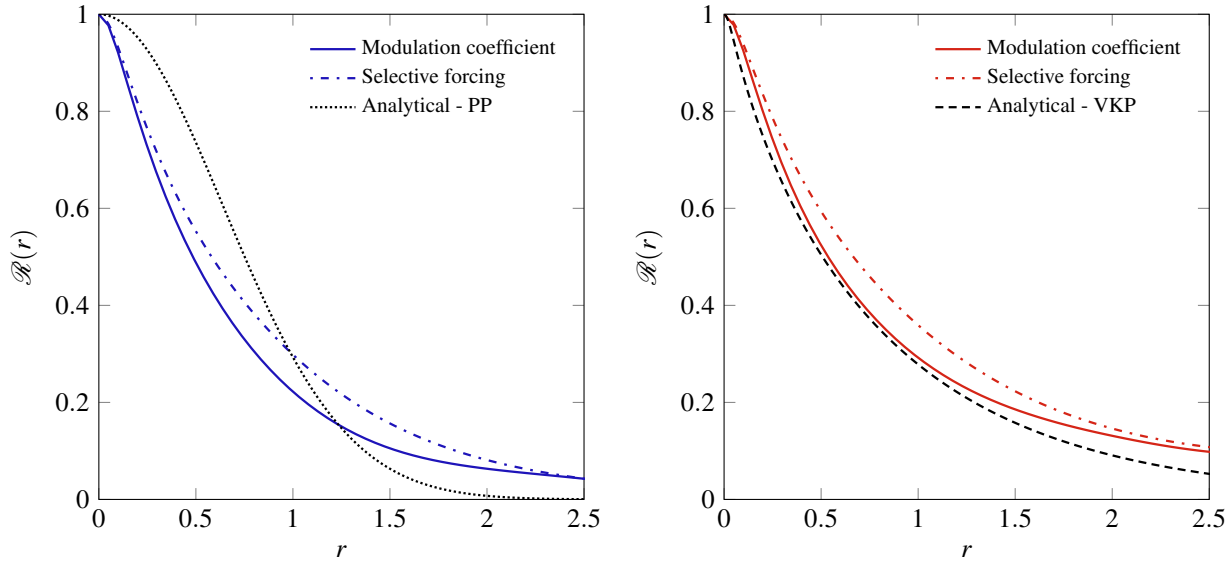

(a) (b)

FIG. 5: Mean longitudinal correlation functions taken over the three directions and averaged over the period of time $t \in [8T : 80T]$. Left: prescribed Passot-Pouquet (PP) energy spectrum. Right: prescribed von Kármán-Pao (VKP) energy spectrum.

lack of energy compared to selective forcing cases. The behavior of the forced PP spectrum with modulation coefficient needs particular attention. First, the maximum occurs nearly at the same wave number k_e as the analytical PP spectrum. However it is observed that an inertial subrange is recovered whereas none are prescribed. This desirable outcome is due to the non linearities of the Navier-Stokes equations. The two spectra resulting from the selective forcing are characterized by a small break near the beginning of the inertial subrange. The "$-5/3$" slope is also recovered for both prescribed spectra. These results suggest that regardless of the imposed spectrum resulting spectra tends towards a more physical behavior, well described in this case of HIT by the VKP spectrum.

As shown in Fig. 4a, the proposed forcing with the modulation coefficient drives the resolved kinetic energy towards different stationary values depending on the prescribed energy spectrum. More energy is recovered when using a PP energy spectrum rather than with VKP energy spectrum. This may be due to confinement effect regarding the VKP spectrum. The empirically choice of β leads to underestimate by 5% the resolved kinetic energy in the "Modulation coefficient - PP" case. For a prescribed VKP energy spectrum, the primary loss of kinetic energy due to confinement effect along with the rough approximation of β leads to an under-estimate by 20% of the resolved kinetic energy. In contrast to the modulation coefficient, the selective forcing drives the resolved kinetic energy towards its target value for both prescribed energy spectra. This approach also removes oscillations and shortens the transient time. These results are suitable to recover better statistical properties which could be taken only after one turnover time scale T.

The longitudinal correlation functions are shown in Fig. 5a and Fig. 5b respectively for a prescribed PP and VKP energy spectrum. Two-point correlation functions are highly dependent on the energy spectrum model. In HIT, an analytic relationship between the energy spectrum and the longitudinal correlation function can be derived[27,28] and is expressed as:

$$U_{rms}^2 f(r,t) = 2\int_0^\infty \left(\frac{\sin \kappa r}{\kappa^3 r^3} - \frac{\cos \kappa r}{\kappa^2 r^2}\right) E(\kappa,t) d\kappa \qquad (37)$$

in which r represents the space separation. This relation is used to plot the analytical PP and VKP correlation functions. We must first recognize that all the functions appear to tend towards the analytical two-point correlation function calculated with a VKP spectrum. This result is in agreement with the obtained spectra since they almost all match the analytical VKP spectrum. In detail, when imposing a PP spectrum with the modulation coefficient (Fig. 5a) the resulting spatial correlations tend to follow the VKP longitudinal function for small distance separations r. The deviation between $0.5m$ and $2.5m$ may be attributed to the different descriptions of large scales between the corresponding spectra as shown in Fig. 4b. The two-point correlation function from the simulation with the modulation coefficient and a prescribed VKP spectrum follows similar trends as the analytical one. The spread between the origin and $1.5m$ is about 6%. For both prescribed spectrum, the selective forcing approach entails a shift towards higher correlation values comparing to modulation coefficient simulations.

To show that the resulting length scales are independent of the domain size, two different length scales $L_{||} = 8\%L_{box}$ and $L_{||} = 19\%L_{box}$ are tested in addition to the studied length scale $L_{||} = 13\%L_{box}$. Simulation parameters are given in Table III. Fig. 6a and Fig. 6b represent the time evolution of the lon-

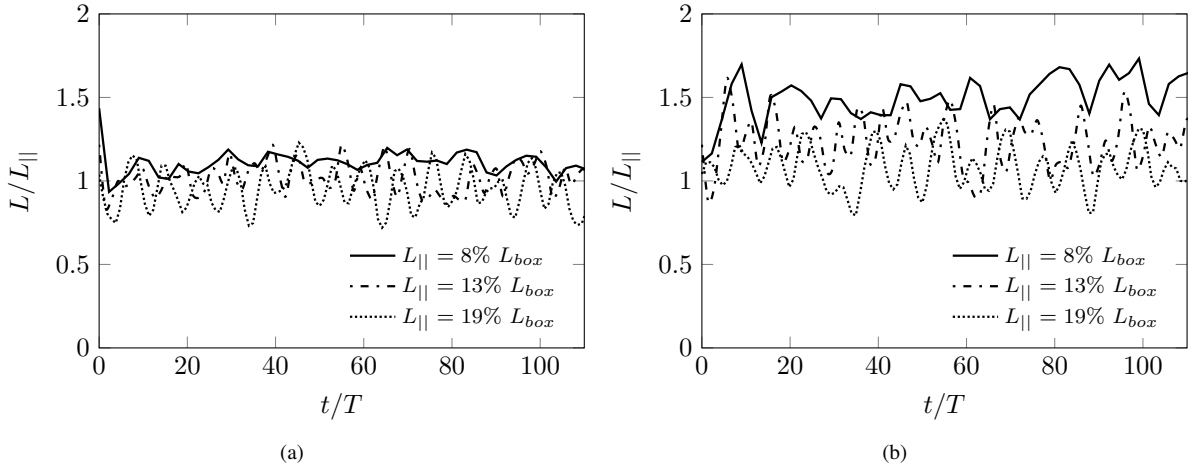

FIG. 6: Time evolution of the longitudinal length scale for three different prescribed integral length scales $L_{||}$. (a) Prescribed Passot-Pouquet energy spectrum, (b) prescribed von Kármán-Pao energy spectrum.

gitudinal length scale for these three cases using the selective forcing approach. This result highlights that the resulting length scales are independent of the domain size, sidestepping the main shortcoming of Lundgren's method[10]. Nevertheless, for both prescribed spectrum, decreasing the prescribed length scale leads to an increase of the resulting length scale, particularly significant for prescribed VKP spectra Fig. 6b. Last, the transverse integral scale is approximately equal to half the longitudinal integral scale complying with HIT conditions. This result is highlighted in Fig. 7 in which longitudinal $f(r)$ and transverse $g(r)$ correlation functions are plotted for the studied case and a prescribed VKP spectrum. The analytical function $f(r)$ is given by Eq. (37) and a similar expression can be obtained for $g(r)$[27,28]. In the present case, the ratio between the resulting longitudinal and transverse integral scales is about 2.1.

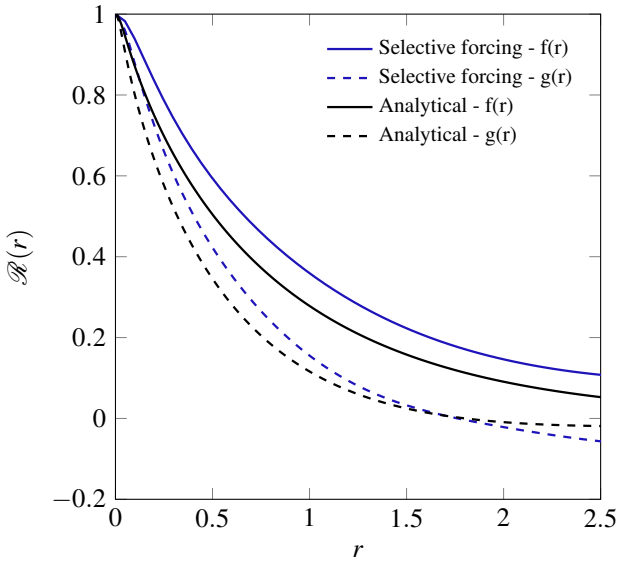

FIG. 7: Mean longitudinal $f(r)$ and transverse $g(r)$ correlation functions taken over the three directions and averaged over the period of time $t \in [8T : 80T]$ for the selective forcing with a prescribed VKP spectrum.

The proposed approach allows to recover length scales that are independent of the domain size. For all cases, the choice of the spectrum seems to affect only large scale while the inertial subrange is recovered. The choice of the β coefficient is significant for modulation coefficient simulations and leads to an under-estimate of the resolved kinetic energy, magnified by confinement effect in the case of a prescribed VKP specrum. In contrast, the selective forcing approach allows to recover the targeted kinetic energy within a short period of time and with a much less oscillating behavior, thereby removing the effects of the β approximation. However, this method leads to an overestimate of longitudinal integral scales, especially in the case of a prescribed VKP spectrum. Finally, the resulting two-time correlation functions, not shown in this section, have an oscillating behavior which is highly non-physical. In the next section, we focus exclusively on the selective forcing approach and a stochastic frequency is introduced to damp oscillations of the two-time correlation function.

2. *Stochastic frequency*

The stochastic part of Eq. (18) is used for the Gaussian distribution of λ. Fig. 8 shows the two-time correlation functions comparing the deterministic cases with the stochastic ones for the selective forcing approach. The analytical two-time correlations expressed in Eq. (17) are similar considering either a PP or VKP energy spectrum, thus only the two-time correlations corresponding to a prescribed PP spectrum are plotted in Fig. 8. We recall here that imposing a deterministic frequency means introducing a non-physical behavior into the computation via the synthetic velocity, *i.e.* strong oscillations of the

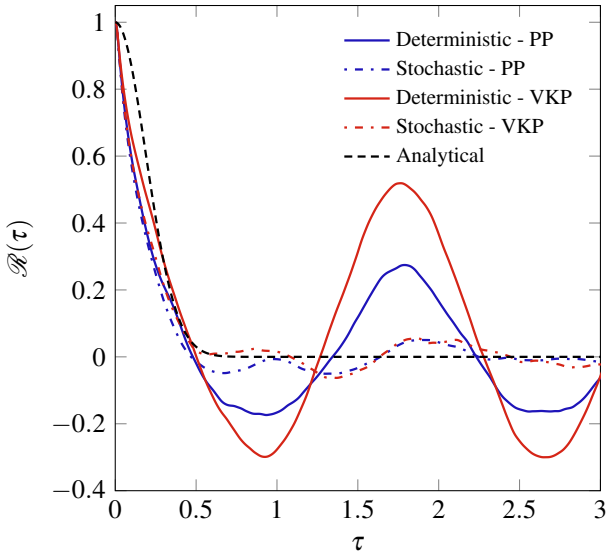

FIG. 8: Two-time correlation function comparison between a deterministic frequency and a stochastic frequency using the selective forcing approach for the two prescribed energy spectrum: Passot-Pouquet (PP) and von Kármán-Pao (VKP) energy spectrum.

theoretical two-time correlation function as shown in Fig. 2. For deterministic cases, this effect is tempered reducing by a factor five for a prescribed PP spectrum and a factor two for a prescribed VKP spectrum oscillations amplitude of the resulting two-time correlations. For small time separation τ the two-time correlation functions follow the same trends for both prescribed energy spectrum. Given a stochastic frequency it is noticeable that oscillations are drastically reduced. Correlation functions are also very similar before vanishing. This confirms that the randomness of the frequency aims only at suppressing oscillations. The fact that small oscillations are still present may be due to the limited number of modes. Indeed, increasing the mode number theoretically leads to better statistics and smooth the two-time correlation related to the synthetic velocity. Simulations with $N = 1000$ modes were performed without any significant improvement (not shown here). Even though, the CPU cost increases drastically when using large number of modes. Therefore, a compromise has to be found between CPU time issues and the layout of the two-time correlation function.

Applying a stochastic frequency to the synthetic velocity gives the desired effect, *i.e.* prevents from oscillations of two-time correlations. However, one needs to ensure that statistical properties such as energy spectrum and two-point correlations remain unchanged. This is done by carrying out a benchmark between the deterministic and the stochastic cases using the selective forcing. The results are not shown here because only minor differences have been observed between the two cases regarding energy spectra and two-point correlation functions. As expected and shown by Eq. (35), the use of a stochastic frequency modifies the amount of energy injected at each wavelength. Naturally, this slightly affects the energy containing part of the resulting spectra, *i.e.* large scales. Accordingly, the two-point correlations are altered but with minor modifications.

C. Influence of grid resolution

In this section, the selective forcing is assessed at various grid resolutions. This sensitivity study is performed by examining some of the well-known most important features occurring in the inertial subrange of HIT. In order to ensure a clearly defined inertial subrange, we consider the case of an inviscid flow. The same numerical parameters as before are used except for the subgrid model. A Smagorinsky subgrid model is employed with a Smagorinsky constant $C_s = 0.148$[14]. Simulations are performed for three additional grid resolutions $N^3 = 64^3$,$N^3 = 96^3$ and $N^3 = 192^3$ besides the studied grid resolution $N^3 = 128^3$.

Among the important features, we examine energy spectra and two-point correlations that are plotted respectively in Fig. 9a and Fig. 9b. Energy spectra are in good agreement with Kolmogorov's "$-5/3$" power-law for all grid resolutions. The results show that the inertial subrange remains almost not affected by the selective forcing. Fig. 9b emphasizes a grid convergence of the two-point correlation functions for small distance separations, for values below $0.5m$. In this region, a similar trend between the four meshes can be drawn, which can be related to the very similar inertial subranges recovered for all spectra. As a remark, discrepancies observed in the two-point correlations at larger r values may come from energy spectra variations observed at low wave numbers in Fig. 9a. A thorough investigation of the influence of grid resolution is beyond the scope of this paper. However, it established that two main features of HIT are preserved.

D. Towards more realistic frequencies

The reconstruction approach coupled with the inverse Fourier method allows some degrees of freedom on the physics that is injected into the computation. The spectrum model as well as the frequency formulation have to be specified and can therefore be adjusted to the physical problem of interest.

As mentioned in Section I, the *straining* hypothesis assumes that large scale frequencies only depend on eddy size and energy. This aspect is spurring us to apply the *straining* hypothesis when forcing at low wave numbers, *i.e.* at large scales. Then, in this section, a frequency following the *straining* hypothesis is assessed. The frequency ω_n reads as:

$$\omega_n = \lambda_n \sqrt{\kappa_n^3 E(\kappa_n)} \tag{38}$$

This frequency formulation is also tested upon HIT in a 2π-triply periodic box, using the same physical and numerical parameters as in IV A. The random variable λ follows the same as before Gaussian distribution $\lambda \sim \mathcal{N}(0.6, 0.8)$. Considering a mode dependent frequency, Eq. (35) must be modified.

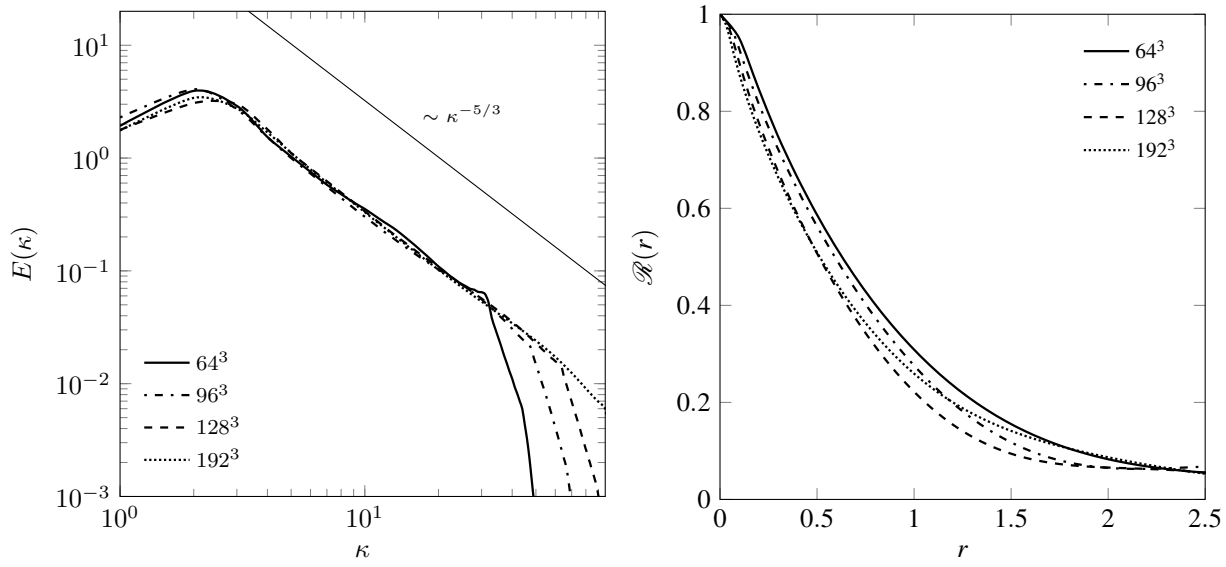

FIG. 9: Comparison between four grid resolutions $N^3 = 64^3$, $N^3 = 96^3$, $N^3 = 128^3$ and $N^3 = 192^3$ for the selective case with a prescribed PP spectrum and a stochastic frequency in the framework of an inviscid flow. a) Energy spectra, b) two-point correlation functions

The turn-over time scale T defined by Eq. (36) is introduced to express the production term P^s from Eq. (29). This leads to the following condition:

$$\sum_{n_s}^{N_c} \hat{u}_n^2 \omega_n^2 = \frac{\varepsilon^\dagger}{2\beta T} + \frac{(k_r^\dagger - k_r(t))}{2\beta T \delta t} \tag{39}$$

in which the coefficient β is still set to 0.5. Fig. 10a shows the time evolution of the resolved kinetic energy. For both prescribed spectra the target value is reached but one can notice that more oscillations of the resolved kinetic energy are observed with a prescribed PP spectrum than with a prescribed VKP spectrum. As shown in Fig. 10b the two spectra present a very similar inertial subrange. At large scales, the maximum of energy is unsurprisingly reached by the prescribed PP spectrum simulation. As expected by the resulting spectrum shape, the outcoming two-point correlation functions are in close agreement. The deviation from the analytical correlation function is about 13% compared to a 26% deviation with a constant frequency. This indicates that prescribing a more realistic frequency also influences statistical properties such as spectra and two-point correlations.

The two-time correlation functions are depicted in Fig. 10d. Besides the small oscillations on their behavior, the two-time correlations are in good agreement with the analytical two-time correlation functions.

V. CONCLUSION

A new forcing technique for eddy-resolving simulations, has been derived, and tested upon homogeneous isotropic turbulence. The proposed forcing technique is based on a reconstruction approach aiming at perturbing the resolved velocity field with a synthetic velocity field. This synthetic component is based on the inverse Fourier method. An energy spectrum must be prescribed which is parametrized by a total kinetic energy and an integral length scale. Regarding control of the resolved kinetic energy, two methods have been proposed: *(i)* one based on a modulation coefficient and *(ii)* a second based on first principle consideration allowing a dynamic control. The latter turns out to be more efficient, since it allows a fast and accurate convergence of the resolved kinetic energy towards its target value. Moreover, the proposed approach overcomes the main drawback of linear forcing methods by providing an unconstrained integral length scale. Furthermore, the use of a stochastic frequency allows to recover more realistic two-time correlation functions by damping oscillations on their behavior.

A significant advantage of this approach is its versatility. For instance, the spectrum model is problem dependent and hence can be adjusted. The time frequency also needs to be specified and can therefore be adapted depending on whether the forcing takes place at high or low wave numbers. The use of a more realistic frequency as the *straining* assumption seems well suited for the forcing of homogeneous isotropic turbulence and also improves the resulting two-point correlations. This approach is easily adaptable to anisotropic homogeneous turbulence by the use of a Cholesky decomposition.

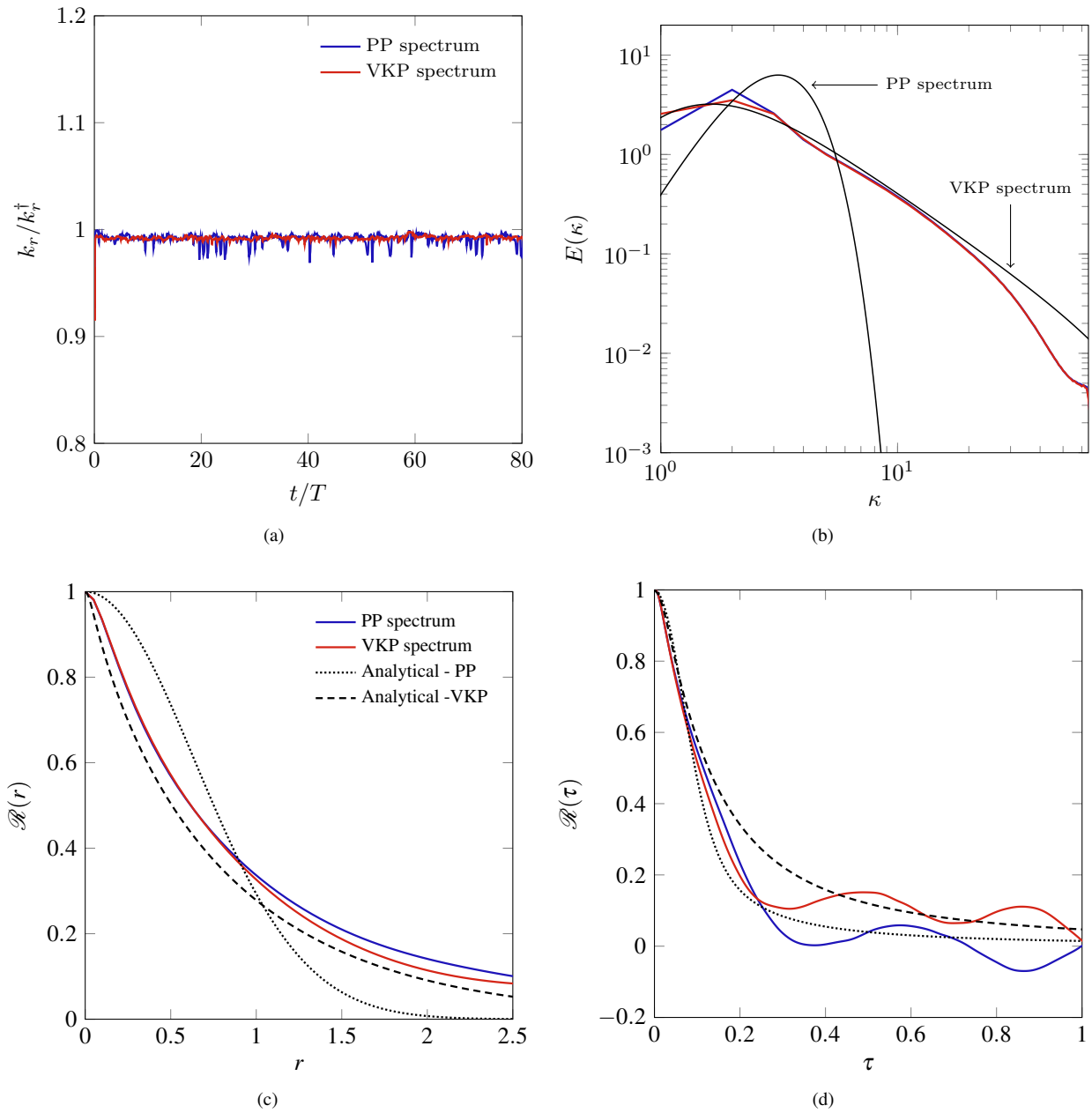

FIG. 10: Comparison between a prescribed PP and VKP spectrum for a selective forcing at low wave numbers with a stochastic *straining* frequency. (a) Time evolution of the kinetic energy, (b) energy spectra, (c) two-point correlation functions and (d) two-time correlation functions.

DATA AVAILABILITY

The data that supports the findings of this study are available within the article.

[1]M. Bassenne, J. Urzay, G. Park, and P. Moin, "Constant-energetics physical-space forcing methods for improved convergence to homogeneous-isotropic turbulence with application to particle-laden flows," Phys. Fluids **28**, 035114 (2016).

[2]M. Bassenne, J. Urzay, K. Schneider, and P. Moin, "Extraction of coherent clusters and grid adaptation in particle-laden turbulence using wavelet filters," Phys. Rev. Fluids **2**, 054301 (2017).

[3]M. Klein, N. Chakranorty, and S. Ketterl, "A comparison of strategies for direct numerical simulation of turbulence chemistry interaction in generic planar turbulent premixed flames," Flames. Flow Turbulence Combust **99**, 955–971 (2017).

[4]B. Bobbitt, S. Lapointe, and G. Blanquart, "Vorticity transformation in high karlovitz number premixed flames," Physics of Fluids **28**, 015101 (2016).

[5]S. Schmidt and M. Breuer, "Source term based synthetic turbulence inflow generator for eddy-resolving predictions of an airfoil flow including a laminar speration bubble," Compt & Fluids **146**, 1–22 (2017).

[6]G. D. Nayer, S. Schmidt, J. Wood, and M. Breuer, "Enhanced injection method for synthetically generated turbulence within the flow domain of eddy-resolving simulations," Computers Mathematics with Applications **75 (7)**, 2338–2355 (2018).

[7] V. Eswaran and S. B. Pope, "An examination of forcing in direct numerical simulations of turbulence," Computers Fluids **16**, 257–278 (1988).
[8] K. Alvelius, "Random forcing of three-dimensional homogeneous turbulence," Physics of Fluids **11**, 1880–1889 (1999).
[9] A. Spille-Kohoff and H.-J. Kaltenbach, "Generation of turbulent inflow data with a prescribed shear-stress profile, third afosr international conference on dns/les arlington, tx," DNS/LES Progress and Challenges (5-9 August 2001).
[10] T. Lundgren, "Linearly forced isotropic turbulence," Annual Research Brief (Center for Turbulence Research, Standford) , 461–473 (2003).
[11] P. Carroll and G. Blanquart, "A proposed modification to Lundgren's physical space velocity forcing method for isotropic turbulence," Phys. Fluids **25**, 105114 (2013).
[12] B. de Laage de Meux, B. Audebert, R. Manceau, and R. Perrin, "Anisotropic linear forcing for synthetic turbulence generation in large eddy simulation and hybrid RANS/LES modeling," Phys. Fluids **27**, 035115 (2015).
[13] J. A. P. Jr. and O. Desjardins, "Technique for forcing high reynolds number isotropic turbulence in physical space," Physical Review Letters **3**, 034605 (2018).
[14] P. Sagaut, *Large Eddy Simulation for Incompressible Flows* (Springer-Verlag, Berlin/New York, 2004).
[15] M. Klein, A. Sadiki, and J. Janicka, "A digital filter based generation of inflow data for spatially-developing direct numerical or large-eddy simulations," J. Comput. Phys. **186**, 652–665 (2003).
[16] R. Kraichnan, "Diffusion by a random velocity field," Phys. Fluids **13**, 22 (1970).
[17] J. Fung, J. Hunt, N. Malik, and R. Perkins, "Kinematic simulation of homogeneous turbulence by unsteady random fourier modes," J. Fluid Mech **236**, 281–318 (1992).
[18] C. Bailly, P. Lafon, and S. Candel, "A stochastic approach to compute noise generation and radiation of free turbulent flows," AIAA Paper , 95–092 (1995).
[19] B. Favier, F. Godeferd, and C. Cambon, "On space and time correlations of isotropic and rotating turbulence," Phys. Fluids **22**, 015101 (2010).
[20] R. Laraufie, S. Deck, and P. Sagaut, "A dynamic forcing method for unsteady turbulent inflow condition," Journal of Compt. Phys. **230**, 8647–8663 (2011).
[21] C. Rosales and C. Meneveau, "Linear forcing in numerical simulations of isotropic turbulence: Physical space implementations and convergence properties," Phys. Fluids **17**, 095106 (2005).
[22] W. Béchara, C. Bailly, , and P. Lafon, "Stochastic approach to noise modeling for free turbulent flows." AIAA Journal **32(3)**, 281–318 (1994).
[23] P. Flohr and J. Vassilicos, "A scalar subgrid model with flow structure for large-eddy simulations of scalar variances," Journal of Fluid Mechanics **407**, 315–349 (2000).
[24] A. Lafitte, T. L. Garrec, C. Bailly, and E. Laurendeau, "Turbulence generation from a sweeping-based stochastic model," AIAA Journal **52**, n°2 (2014).
[25] "P^2REMICS collaborative website," https://gforge.irsn.fr/gf/project/p2remics/.
[26] F. Boyer, F. Dardalhon, C. Lapuerta, and J.-C. Latché, "Stability of a crank-nicolson pressure correc-tion scheme based on staggered discretizations," International Journal for Numerical Methods in Fluids **74**, 34–58 (2014).
[27] J. O. Hinze, *Turbulence* (McGraw-Hill, 1975).
[28] P. Sagaut and C. Cambon, *Homogeneous Turbulence Dynamics* (Springer International Publishing AG, 2018).
[29] G. Mallouppas, W. K. George, and B. G. M. van Wachem, "New forcing scheme to sustain particle-ladenhomogeneous and isotropic turbulence," Phys. Fluids **25**, 083304 (2013).